Journal of Applied Physics ARTICLE pubs.aip.org/aip/jap

Defect dynamics in the presence of excess energetic carriers and high electric fields in wide-gap semiconductors

Cite as: J. Appl. Phys. **135**, 195701 (2024); doi: 10.1063/5.0203047
Submitted: 8 February 2024 · Accepted: 30 April 2024 ·
Published Online: 16 May 2024

View Online Export Citation CrossMark

Andrew O'Hara,[1,2] Ronald D. Schrimpf,[3] Daniel M. Fleetwood,[1,3] and Sokrates T. Pantelides[1,3,a)]

AFFILIATIONS

[1]Department of Physics and Astronomy, Vanderbilt University, Nashville, Tennessee 37235, USA
[2]Department of Physics, Western Michigan University, Kalamazoo, Michigan 49008, USA
[3]Department of Electrical and Computer Engineering, Vanderbilt University, Nashville, Tennessee 37235, USA

[a)]**Author to whom correspondence should be addressed:** pantelides@vanderbilt.edu

ABSTRACT

Irradiation of semiconductors by energetic beams generates excess electrons and holes and may cause device degradation or failure. Both gradual degradation by total ionizing radiation (TID) and sudden degradation/failure (soft/hard breakdown) by a combination of energetic heavy ions and high voltages (typically single-event effects or SEEs) are mediated by excess carriers. The role of defect dynamics in TID degradation has been adequately understood by a combination of experiments and density-functional-theory (DFT) quantum calculations, but little has been done so far to document a role for ion-induced defects in SEE. Here, we report proof-of-principle DFT calculations in a model cubic GaN system for two defect-related excess-carrier phenomena that can play a role in various forms of device degradation and failure. The first phenomenon is the existence, dynamics, and potential roles of defect-induced quasi-localized "resonant states" in the energy-band continua. These states can enhance TID-excess-carrier and hot-carrier degradation. Furthermore, they evolve and multiply during energetic-ion-induced atom recoils and defect creation (displacement damage) and can potentially serve as excess-carrier conduction paths in SEE. The second phenomenon is the conversion of isolated vacancies into nanovoids that can participate in the formation of conducting defect "nanowires" dressed by resonances or in explosive SEE hard breakdowns.

© 2024 Author(s). All article content, except where otherwise noted, is licensed under a Creative Commons Attribution (CC BY) license (https://creativecommons.org/licenses/by/4.0/). https://doi.org/10.1063/5.0203047

18 May 2024 05:49:24

I. INTRODUCTION

Excess electron–hole pairs can be introduced in semiconductor devices by radiation such as x rays, electrons, protons, ions, and lasers in both space and terrestrial environments. Total ionizing dose (TID), in the context of device degradation, refers to the cumulative long-term degradation of a device when exposed to radiation. The primary effect of TID irradiation is to generate excess electron–hole pairs (little or no displacement damage). High-energy carriers thermalize to lower energies, losing energy by a variety of processes.[1–4] At relatively low energies, excess carriers, like hot electrons, can activate pre-existing benign defects, e.g., by enabling the release of passivating hydrogen atoms via various atomic-scale mechanisms.[5–15] The activated defects can be charged, thereby impacting critical device properties such as the threshold voltage and the transconductance. Much of the detailed understanding of the atomistic mechanisms was obtained by a combination of electrical measurements, low-frequency 1/*f* noise measurements, and density-functional-theory (DFT)-based quantum calculations.[10–15] In the presence of large external voltages, as in power devices, carriers are continuously accelerated to higher energies. If the carriers acquire enough energy to generate additional electron–hole pairs, avalanche breakdown can occur.[16]

Very different processes lead to the sudden degradation (soft breakdown) and sudden failure (hard breakdown) of electronic devices when irradiated by energetic ion beams. These phenomena can be triggered by the passage of a single energetic ion through a dielectric layer or a lightly doped semiconducting layer that is biased at an electric field well below the electrical breakdown limit (single-event effects or SEEs).[17–23] Single-event gate rupture (SEGR) and

© Author(s) 2024

single-event burnout (SEB) are common SEE failure modes that are initiated by excess carriers generated by the striking ion and the energy transferred to the device by the ion (linear energy transfer or LET) and by the applied voltage.[17,19,24–33] In both cases, the device failure is attributed to the formation of a highly conducting "electron plasma wire" along the path of an ion strike. A role for the multitude of defects (displacement damage or DD) that are generated by the energetic ions is not usually invoked to channel or enable this plasma wire. Pits and voids, are, however, present after hard breakdowns,[34–37] which may be viewed as an indication for possible DD channeling the plasma wire. A role for ion-beam-induced defects in soft breakdowns has been proposed. For example, a detailed DFT-based study of defect formation along the ion path in a SiO_2 layer led to calculated currents in the range of experimental data for radiation-induced soft breakdown.[26,38,39] A similar possible mechanism for soft breakdown prior to a SEB occurrence was recently suggested in the case of ion irradiation of β-Ga_2O_3 Schottky diodes under high applied voltages.[40] In this case, the migration of charged ion-beam-generated defects[41] such as vacancies and interstitials under the high applied bias was invoked to explain a sudden rise of current to levels that are much higher than normal, but still below breakdown, followed by continuing, enhanced conduction along a stable, defect-mediated pathway.

At a fundamental level, the presence of excess electrons and holes has long been known to have major implications on defect dynamics, most notably recombination-enhanced defect migration.[42,43] An electron in the conduction bands can drop into a defect level in the energy gap and from there it can annihilate a hole in the valence band, releasing a whole bandgap of energy into the lattice by multiphonon processes. This local heating enables enhanced migration over energy barriers. The phenomenon, including effective athermal migration at cryogenic temperatures, has been well documented by both experiments and theory.[44–50]

In this paper, we report proof-of-principle DFT-based theoretical investigations of several hitherto unexplored phenomena that can occur when excess or hot carriers are present in a semiconductor and can participate in radiation- and hot-carrier-induced degradation and failure. Calculations are performed for a model cubic GaN system. We first document the existence of defect-induced "resonances" in the band continua, namely, quasi-localized states and analogs of the bound states in the energy gap. These states are called resonances because they behave like Bloch states at some distances far from the defect; hence, they are resonant in energy with Bloch states of the perfect crystal. Such resonances were first documented by DFT calculations in 1978,[51] but possible effects on defect dynamics or other consequences have not been investigated. Here, we report procedures to enable the identification of defect-induced resonances in DFT calculations. These resonances can enhance both TID- and hot-carrier device degradation by enhancing H-release from passivated defects and by enhancing carrier capture by activated defects. We further show that, during defect reconfigurations, resonances evolve and can multiply in numbers, which suggests that, during defect creation by energetic ions, the ion path is dressed by evolving and multiplying resonances that can serve as highly conducting paths for excess carriers, potentially playing a significant role in SEE device breakdown. We also demonstrate that occupation of resonances by excess or hot carriers reduces the defect total energy and the capture of such carriers at states in the bandgap can significantly enhance the ability of defects to reconfigure and migrate. In the second part of the paper, we demonstrate that the energy to remove nearest-neighbor atoms of pre-existing, depassivated, or ion-beam-induced vacancies to interstitial sites can be significantly lower than the energy to remove atoms from perfect-lattice to interstitial sites. As a result, Frenkel-pair (FP) creation adjacent to vacancies can be enhanced significantly. Repetition of such events at a vacancy amounts to a "defect multiplication process" and nanovoid growth. When the atom-removal energies are of the same order as the bandgap, recombination-enhanced void growth can take place and be further enhanced by excess carriers in resonances. Depassivated vacancies under TID conditions can, therefore, grow into nanovoids that can act as carrier traps and scattering centers, potentially complicating data analysis. Under SEE conditions, the energy for void growth can be provided by Joule heating generated by the applied voltage and to a lesser extent by the ion LET, while the multitude of dangling bonds along with the accompanying resonances can provide excess-carrier conducting paths for soft breakdowns. At extremely high Joule-heating levels, runaway void growth may induce a hard breakdown, featuring pits and voids, as observed.[34–37] The energetics of void growth under irradiation in different wide-gap semiconductors may serve as a criterion for radiation hardness.

II. COMPUTATIONAL METHODOLOGY

All calculations were performed using density functional theory with the Vienna *ab-initio* simulation package (VASP)[52] utilizing the project-augmented wave (PAW) method,[53,54] the Perdew–Burke–Ernzerhof version of the generalized gradient approximation,[55] and a plane-wave cutoff of 400 eV. For the present purposes, with emphasis on total energies as opposed to eigenenergies, the PBE exchange-correlation functional is both suitable and computationally practical. Calculations were performed for defects in cubic GaN as a model system for which the computational complexity is lower than in wurtzite GaN. In order to simplify the geometry of transition states for simple defect migration, e.g., a Ga vacancy, a $4 \times 4 \times 4$ supercell of the conventional cubic GaN unit cell containing 512 atoms was used for all calculations and the Brillouin zone was sampled at the Γ point. In the cubic GaN phase, symmetry constraints force the vacancy-migration transition state to metastably balance between stable vacancy sites allowing for easier reoptimization of the structure within the constrained-occupation DFT calculations. Nudged-elastic band calculations[56,57] confirm that this is the correct transition state geometry. For structural optimization, forces were converged to be less than 0.01 eV/Å per atom. To simulate the presence of electron–hole pairs, we performed spin-polarized constrained-occupation DFT calculations in which both holes and electrons are explicitly included so that the net charge of the supercell is always zero. For the energetics of defect multiplication processes, calculations of successive FP creations were performed for neutral supercells without spin-polarization for computational efficiency as the voids are enlarged.

18 May 2024 05:49:24

© Author(s) 2024

III. RESONANT STATES WITHIN THE BAND CONTINUA

The prototypical example of a resonant state is the a_1 level of vacancies in tetrahedral semiconductors such as silicon and the III-V semiconductors. In the absence of symmetry-lowering relaxations, the dangling bonds on the vacant site's four nearest neighbors combine to anchor the formation of a non-degenerate s-like a_1 and a triply degenerate t_2 energy level. The latter is well known to be a localized state in the energy gap and can be split by Jahn–Teller distortions depending on its occupation. Electron-paramagnetic-resonance data from defects in electron-irradiated Si data enabled G. D. Watkins to identify the vacancy in Si in the 1960s.[58] DFT calculations later showed that the a_1 level resides inside the valence bands as a resonant level.[51] While residing inside the valence bands, this level retains a strong degree of localization despite being hybridized with band states. The calculations reported in Ref. 51 also found that an additional vacancy-induced a_1 resonance exists within the valence bands of Si. In our present model system, i.e., a Ga vacancy in c-GaN, we find that the a_1 resonance is spin polarized with one of the spin states very close to the valence-band edge and moves into the bandgap quickly as the vacancy-migration process begins. Similarly, the spin-splitting of the t_2 level forces the occupied spin-majority sites into the valence band while leaving the unoccupied spin-minority states localized in the energy gap. We will focus our attention on the conduction-band region and use the atomic reconfigurations that occur as the Ga vacancy migrates to an equivalent Ga site to investigate the evolution of the accompanying resonances.

A simple, but tedious, way to identify resonant levels is to look at the charge density (i.e., $|\psi(\boldsymbol{x})|^2$) for each state in the band continua and visually compare their localization with known delocalized band states and perfect-crystal Bloch states. In Fig. 1(a), we show the charge density for the lowest-energy resonant level of the neutral Ga vacancy in c-GaN. In Fig. 1(b), we similarly show the charge density for the lowest-energy resonant level of the transition state configuration for vacancy migration. In relation to the conduction-band edge, the lowest-energy resonant state is much higher in energy for the stable vacancy site (E_{CB}+2.45 eV) compared to the vacancy-migration transition state (E_{CB}+1.40). Furthermore, a significant increase in the localization of the charge density occurs at the transition state.

Naively, one may assume that this localization process is simply a combined localization and downward shift of the same resonant state. However, a thorough investigation of the conduction band states of the transition state geometry indicates that additional resonant levels exist as we will discuss below. Though some resonances may originate from the dangling bonds around a vacancy,[51] e.g., the a_1 resonance near the top of the valence bands, other resonances are simply caused by the defect potential. The evolution of the resonances along the vacancy migration path reflects the changing defect potential as well as changes in bonding configuration. The generation of resonant states by a defect potential is similar to the way that a free-electron plane wave becomes a quasi-localized Whittaker function in the vicinity of a proton in vacuum, depending on its energy.[59,60] During the formation of these resonance levels, we see in several cases [Figs. 1(a), 1(b), 2(a), 2(d), and 4(b)] that, as these resonances form, there is an increased fraction of the wave function of the resonant state within the interstitial regions, suggesting a possible association with the so-called floating states found previously in bulk and defective tetrahedral semiconductors.[61–63]

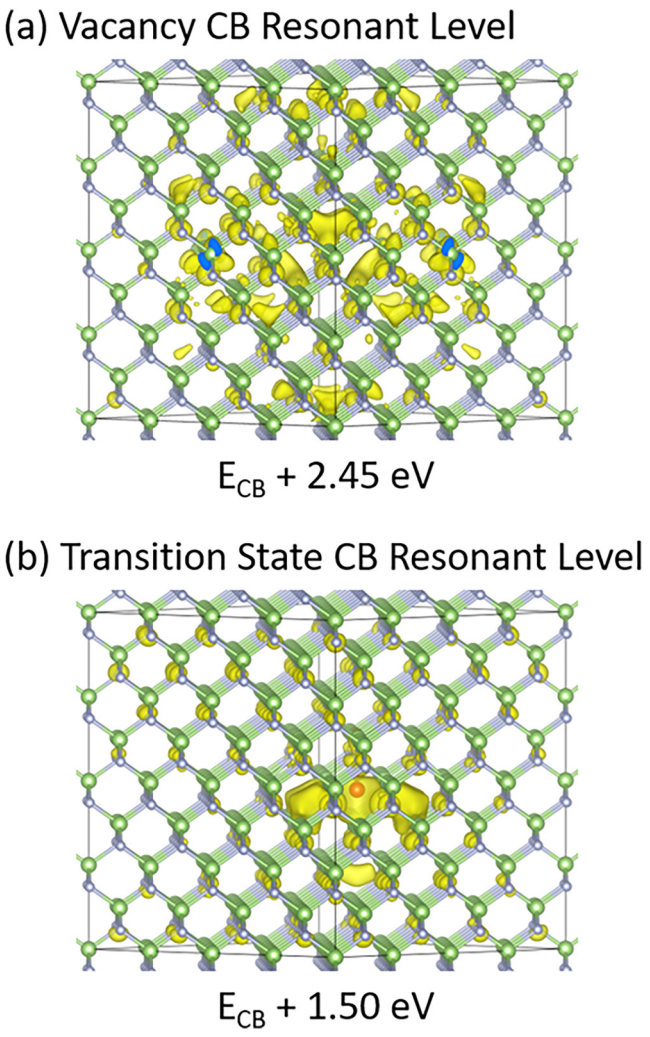

FIG. 1. Charge density (i.e., $|\psi(\boldsymbol{x})|^2$) for the lowest-energy conduction-band resonant state for (a) the stable Ga vacancy site with an isosurface level of 1.3×10^{-4} e Å^{-3} and (b) the migration transition state in c-GaN plotted over the atomic structures with an isosurface level of 1.8×10^{-4} e Å^{-3}.

Due to the diffuse nature of some resonant levels, it is not practical to calculate projected-density-of-states plots for identification of the resonant levels. While one could look at visualizations of the projected charge density of each band in the supercell (as done in Fig. 1, for example), this method is too cumbersome. An alternative approach is to use plots of the relative wavefunction localization on neighboring atoms (i.e., projection of the wave function within a Wigner–Seitz sphere around a given atom) as a function of distance from the defect center. In Fig. 2, we demonstrate

18 May 2024 05:49:24

© Author(s) 2024

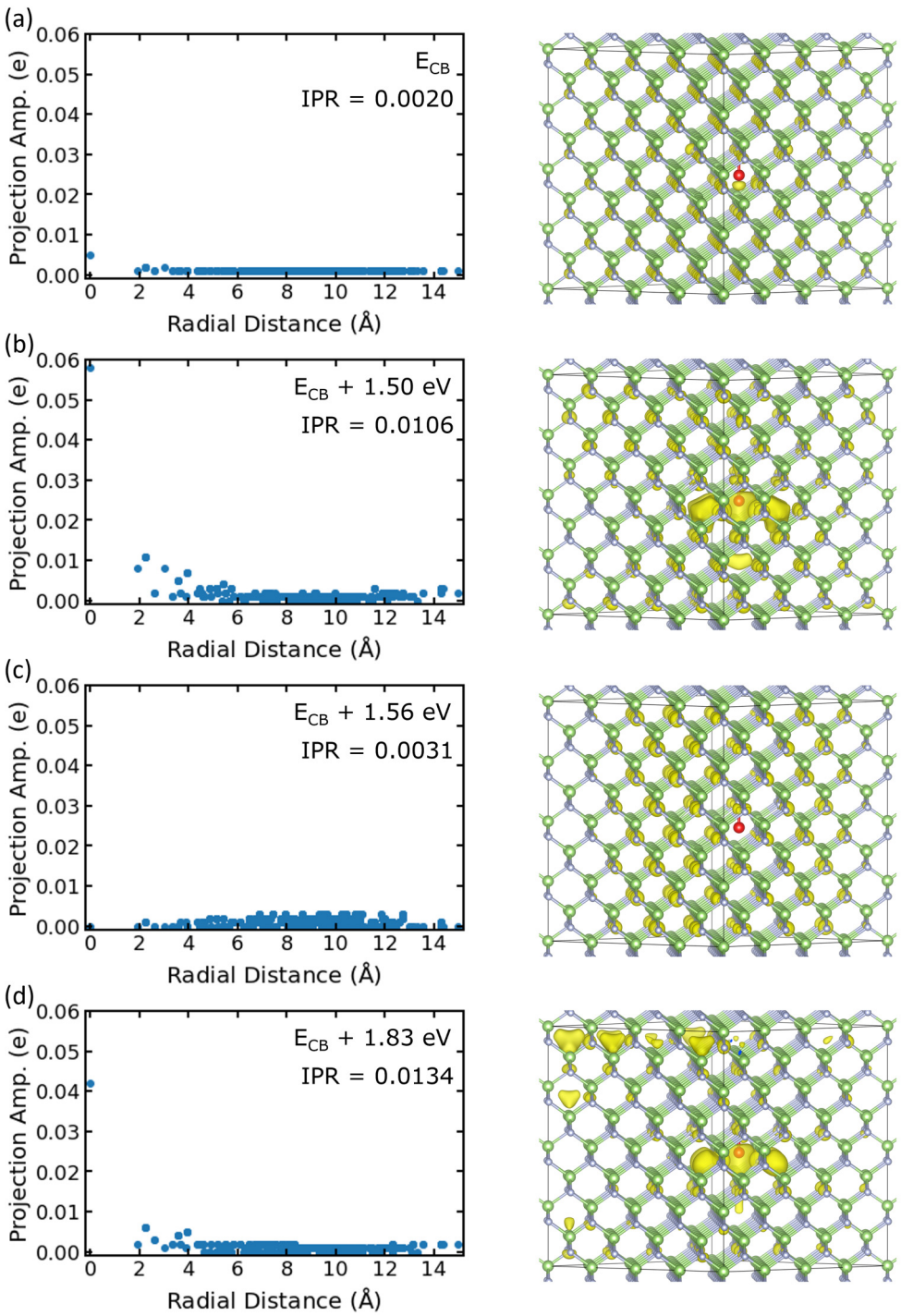

FIG. 2. Wavefunction projection amplitude (within a Wigner–Seitz radius) as a function of distance from the defect centroid and associated charge density (i.e., $|\psi(\boldsymbol{x})|^2$) plot for (a) the conduction band minimum, (b) the first resonant state, (c) the next highest band state, and (d) the second resonant state for the migration transition site of the Ga vacancy in c-GaN. For each plot, the inverse participation ratio (IPR) is listed below the eigenenergy. Due to the resonant levels being more delocalized than traditional midgap defect levels, the tails of the wave functions can lead to overlaps due to periodic boundary conditions in finite supercell calculations, as seen in the upper left of the isosurface plot (right column) of panel (d). All isosurface levels are shown at 1.8×10^{-4} e Å^{-3}.

18 May 2024 05:49:24

© Author(s) 2024

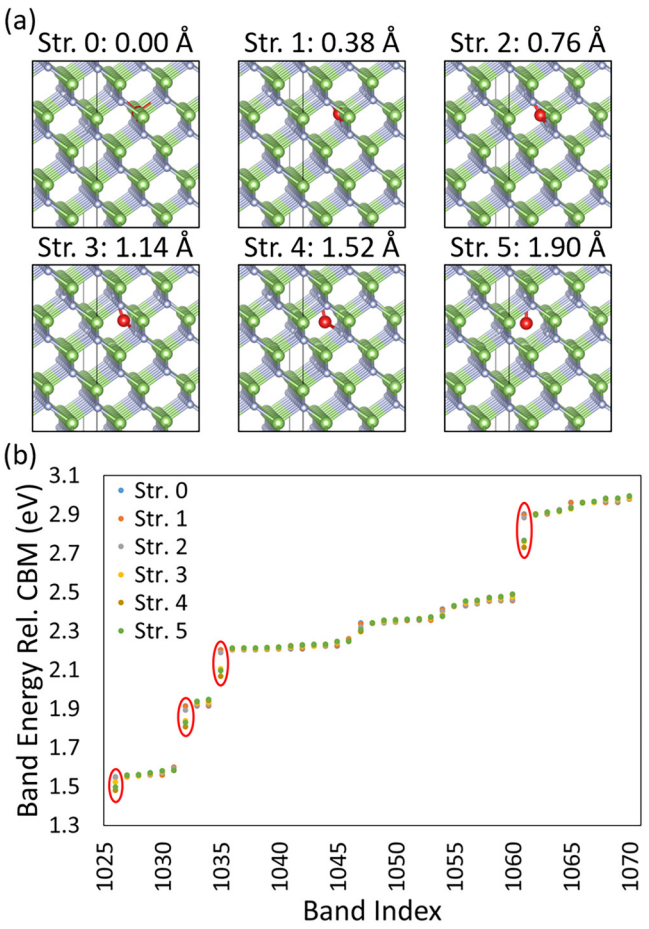

FIG. 3. (a) Structure of the migration process for the Ga atom that moves during vacancy migration in c-GaN between the stable vacancy site and the migration transition state as well as the distance covered by the migrating Ga atom during the movement. (b) Plot of the eigenvalue energies as a function of band index for the lowest 45 states in the present $4 \times 4 \times 4$ supercell of c-GaN. While several states have significant changes in eigenvalue energy, the red circles represent those that are confirmed to be the formation of resonant levels at the migration transition-state structure.

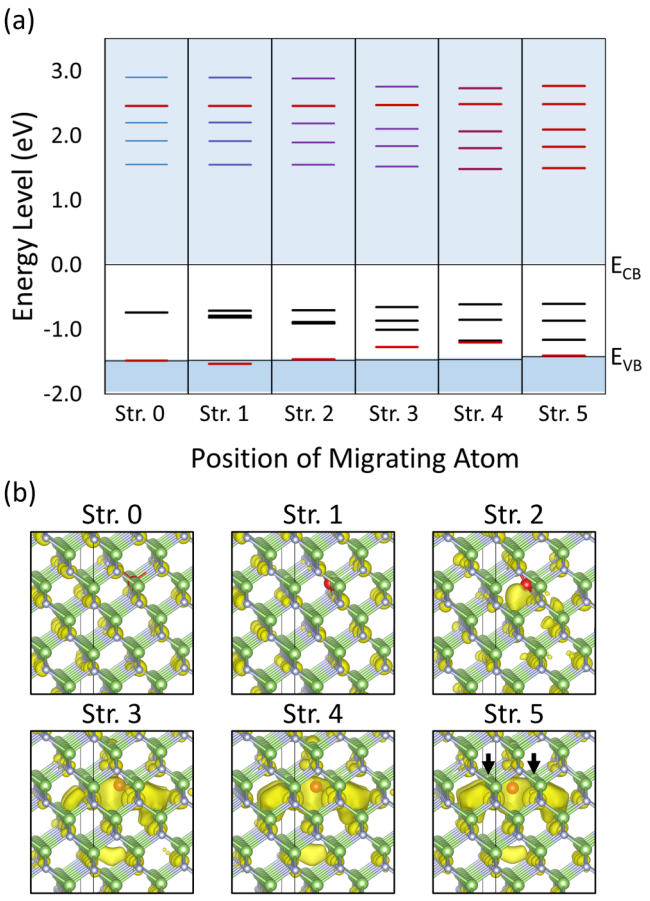

FIG. 4. (a) Summary of the states that form localized resonant levels during the migration process for the spin-minority channel as originally found via the analysis in Fig. 3(a) and their energy evolution. Additionally, the evolution of the unoccupied midgap levels from an initially triply degenerate level to three energetically distinct level is shown. Furthermore, we show that during the migration process, the a_1 resonant level in the spin minority channel crosses from inside the valence band continuum to become a midgap level at the transition state. (b) Evolution of the charge density (i.e., $|\psi(\boldsymbol{x})|^2$) for the lowest-energy resonant state indicating how the localized level forms from an initially delocalized band state as the Ga atom migrates from its stable site toward the transition-state site (initial and final sites are indicated by black arrows in Str. 5). All isosurface levels are shown at 1.8×10^{-4} e Å^{-3}.

this approach in the case of the lowest three eigenstates of the supercell for the vacancy migration transition state: (a) the conduction band edge, (b) the lowest-energy resonant level, and (c) the next band state. These plots show that additional resonant levels exist. For example, there is another resonant level at E_{CB}+1.83 eV in Fig. 2(d), where a similar localization to that of the lower-energy resonant state occurs at the site of the transitioning Ga atom. In principle, such plots allow not only for quicker processing (as the relevant projections can be generated by the DFT package at the end of a calculation), but they can be combined with a minimal cutoff threshold to pre-select energy levels for further analysis. In principle, such a threshold is *ad hoc* and depends upon the specific defect, supercell size, and chosen Wigner–Seitz radii. For the present system, setting the minimal cutoff threshold to any value between 0.01 and 0.04 selects all states found to be resonant levels in this paper (e.g., as discussed in Figs. 2 and 3). In other words, for delocalized levels, no atomic radii contain more than 0.01 of the band and, for quasi-localized levels, at least one atomic radius contains more than 0.04 of the band. As shown in the second column of Fig. 2, the charge-density projections for the pre-screened bands can then be visualized for confirmation of their nature as necessary.

Another approach to screening for resonant levels borrows the concept of the inverse participation ratio (IPR) from the context of Anderson localization.[64,65] Numerically, the inverse participation

18 May 2024 05:49:24

© Author(s) 2024

ratio measures the degree of localization for both vibrational and electronic modes by using the amount of the state localized at different atomic sites in the lattice[66,67] and then performing a sum of squares vs square of sums analysis of the local densities. In the present case, we utilize our projections within the Wigner–Seitz radii and calculate

$$r^{-1} = \left(\sum_{i=1}^{N} p_i^2\right) / \left(\sum_{i=1}^{N} p_i\right)^2, \tag{1}$$

where the p_i are the total projections within each Wigner–Seitz radius and N is the total number of atoms in the supercell. For a delocalized orbital, the IPR calculated by Eq. (1) should be on the order of $1/N$, or slightly higher due to inhomogeneity. For localized and quasi-localized levels, the IPR tends to be significantly higher. In the present work, $N = 511$ and $1/N \approx 0.001\,96$. The nonresonant states in the conduction band are on the order of 0.002–0.004. The resonant levels found in the present work are several times higher, ranging from 0.0085 to 0.0134 for the transition state structure. For comparison, the more localized midgap states of the transition-state structure range from 0.15 to 0.19. Similar to the projection plots, the IPR based on the Wigner–Seitz ratios provides a quick screening tool to search for resonant levels.

To gain further insight into the localization process of the resonant levels, we interpolate the structure along the migration path from the stable vacancy site to the transition state. In Fig. 3, we plot the unoccupied electronic eigenvalues (i.e., "band energies") as a function of their index at the Γ point for the spin minority energy levels; a plot for the spin majority channel looks similar. In general, most of the eigenvalues remain essentially unchanged. However, at several places, there are noticeable changes in the eigenvalue energies of order ∼0.05 to ∼0.14 eV. Further investigation by comparison with the charge-density projections, the projection amplitude plots, or IPR values confirm the existence of five resonant states that are within 3 eV of the conduction band. The first circled level corresponds to the resonant level shown in Figs. 1(a) and 2(b). The second circled level corresponds to the second resonant level found through the projection amplitude vs distance plot in Fig. 2(d).

By tracing out the evolution of the charge-density projection of the above defect configurations, we are able to observe that the new resonant states all begin as delocalized band states and gradually localize as the vacancy migration process proceeds, namely, as a Ga atom moves from its lattice site to the adjacent vacant Ga site, leaving a Ga vacant site behind. We illustrate the general evolution of the resonant levels in Fig. 4(a). For the lowest-energy band state that localizes as the system evolves from the stable vacancy to the migration transition state, we explicitly plot the charge density of the state as the atom moves toward the transition-state site in Fig. 4(b). The localization emerges from an initially delocalized band level, beginning soon after the migrating atom moves halfway between the initial- and transition-state sites. Localization of new resonant levels after partial migration suggests that defect reconfigurations may well host different resonances with different degrees of localization. This finding can be generalized to different defects that feature diverse resonances.

So far, we have only investigated the existence and evolution of resonant states during a prototype sequence of defect reconfigurations and found a substantially rich behavior. The next task is to investigate what can happen if excess carriers are present and potentially occupy resonances. Introducing a few excess electrons and holes in a relatively small supercell can amount to a very large density of excess carriers. In order to ensure that we use a reasonable density of excess carriers, we obtain an estimate as follows. To first order, the typical carrier density of the thermalized e–h pairs generated during an ion strike can be approximated from the ion's linear-energy transfer (LET; L), mass density of the material (ρ), e–h pair creation energy (E_{ehp}), and approximate cross-sectional area of the track (A),[21]

$$n = \frac{L\rho}{E_{ehp}A}. \tag{2}$$

For GaN, $\rho = 6.15$ g/cm^3 and $E_{ehp} = 8.9$ eV.[68] While values for LET can vary over a wide range, space and certain other environments exist in which heavy-ion strikes are possible.[69] A common test source, which represents the midpoint for space environments, is Cf-252 which produces heavy-ion fission fragments with LET values up to 45 MeV cm^2/mg.[40] Typically, cross-sectional diameters are of order 10–100 nm, e.g., often a 50 nm Gaussian is used for Technology Computer-Aided Design (TCAD) simulations.[28] In this particular case, assuming a circular cross section with a 25 nm radius, the average carrier density is 1.6×10^{21} carriers/cm^3. In the present calculations, we utilize a total of six e–h pairs, with both excess valence-band holes and conduction-band electrons explicitly included simultaneously, in the supercell volume (split evenly across spin majority and minority states), which equates to a carrier density of 9.7×10^{20} carriers/cm^3. Therefore, the carrier density that we use in our calculations is in line with the experimental estimates for higher-LET particles and provides flexibility for differing combinations of the occupation of delocalized band states and resonant levels. Furthermore, our choice avoids some numerical-stability issues that arise due to band crossings of unoccupied and occupied levels. When occupying the conduction-band energy levels at each point along the migration path, we retain the same occupations as at the previous point and then relax the structure in order to ensure we get a true change in the total energy. Energy levels move only by a small amount compared with the net relaxations shown in Fig. 5. In each case, we occupy the electronic levels at the conduction band edge and the first subsequently available band states of the supercell. Given the closeness of the resonant level and the delocalized band states, we are able to fill either type and keep all the initially chosen eigenvalues within 0.1 eV or less regardless of whether the lowest resonant state is filled in either spin channel. In a real system, resonances are occupied and unoccupied dynamically so that these calculations represent an instant in time to better understand the contributions to the defect dynamics

One measure is the impact of resonances and their potential occupancy on the total energy of the defect. Prior to the inclusion of e–h pairs in the calculation, the migration energy barrier for the vacancy is 2.62 eV [labeled as "no e–h pairs" in Fig. 5(a)]. When the e–h pairs are included, but no resonant levels are occupied, the

18 May 2024 05:49:24

© Author(s) 2024

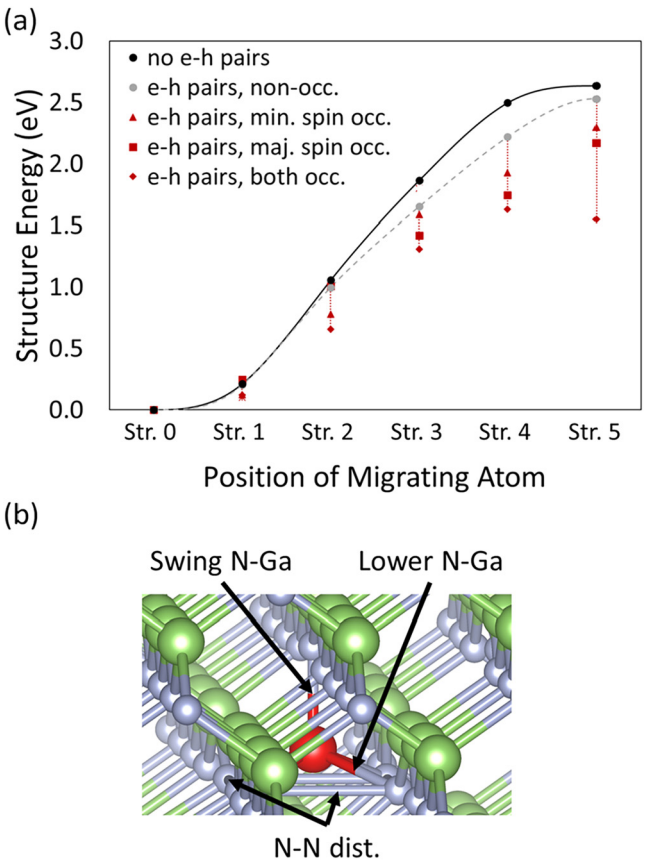

FIG. 5. (a) Energy of the optimized structures along the pathway with no e–h pairs ("no e–h pairs," solid black curve), e–h pairs but no conduction band resonant state occupations ("e–h pairs, non-occ.," dashed gray curve), and various occupations of the low-lying conduction band resonant states. For the occupied resonant states, these are shown for minority spin channel occupation ("e–h pairs, min. spin occ.," red triangle), majority spin channel occupation ("e–h pairs, maj. spin occ.," red square), and occupation of both spin channels ("e–h pairs, both occ.," red diamond). As the atom migrates, the energy along the path may fluctuate in a jagged manner between these extremes as resonant levels are populated and depopulated (in the calculations for the red and gray points of structures 3–5, one of the neutralizing holes is in the a_1 bound state). (b) Enlargement of the atomic geometry surrounding the Ga atom at the transition state illustrating the swing N-Ga bond, the lower N-Ga distances, and both N-N distances, as discussed in the text.

migration energy barrier is 2.54 eV [labeled as "e–h pairs, non-occ." in Fig. 5(a)]. That the two numbers are essentially the same within numerical accuracy confirms that excess e–h pairs that are placed in delocalized band states have no real effect on the vacancy-migration energy barrier. To explore how the total energy of a defect changes when excess carriers occupy resonances, we examine each point on the migration path separately. Each configuration can be thought of as a different defect. Results correspond to a reduction of the migration barrier at that point for the vacancy. These calculations would allow us to also infer the impact of resonance occupancy on the energy profile of the migration barrier only if a particular resonance were occupied along the entire migration path. Though the lifetimes of carriers in a resonance are not easy to estimate, they are not likely to be that long so that the results of these calculations need to be evaluated with that in mind. Below we discuss the controlling factor of these lifetimes and identify a more direct impact on migration barriers.

We now focus our attention on conduction-band resonances, which have a rich and evolving structure as seen in Fig. 4(a). In contrast, the single a_1 resonance in the valence bands is initially very close to the valence-band edge and then quickly crosses into the bandgap as an occupied state so that its effect is fully taken into account in the calculation of the migration energy barrier at T = 0 K. In this paper, we do not consider explicit charge states of the vacancy, i.e., changes in occupation of the midgap states for the range of structures, because we aim to unveil generic effects induced by large electric fields other than the tilting of the barrier, which is well understood, and by excess carriers. From now on, therefore, we consider only the effects of excess electrons occupying conduction band resonances in our model system of the Ga vacancy in cubic GaN.

We calculated the changes in the total energy of the defect that occur at a series of five points along the migration path for several different resonance occupancies to assess the local impact of each individual configuration along the migration path. The results are shown in Fig. 5(a), demonstrating that the impact on the corresponding values of the energy barrier in the absence of excess carriers is quite substantial. The greatest impact occurs at the transition state. We show the results in detail in Table I where we also show the effects of occupied resonances on the distinct local lattice relaxations structure of the transition state. More specifically, at the transition state, there are four primary atomic distances that can be correlated with the change in barrier for the present case. First, there is the swing N-Ga bond that is common to the Ga atom at its

18 May 2024 05:49:24

TABLE I. Summary of the atomic distances as described in Fig. 5 for no e–h pairs and each considered case of occupied conduction-band resonances by excess electrons.

System	Barrier (eV)	Swing N-Ga (Å)	Lower N-Ga (Å)	N-N dist. (Å)
No e–h pairs (i.e., ground state)	2.62	1.90	2.25	3.15, 2.94
No occupation by excess electrons (e–h pairs, non-occ.)	2.54	1.90	2.24	3.11, 2.93
Maj. spin occupation by an electron (e–h pairs, min. spin occ.)	2.19	1.91	2.44	3.39, 3.15
Min. spin occupation by an electron (e–h pairs, maj. spin occ.)	2.30	1.92	2.40	3.32, 3.11
Both occupied by electrons (e–h pairs, both occ.)	1.55	1.94	2.62	3.63, 3.33

© Author(s) 2024

lattice site for either position of the vacancy and to which the Ga atom remains bonded during the entire process. Second, there is the distance from the Ga atom to each of the four nitrogen atoms in the plane below. Lastly, there are the two sets of nitrogen–nitrogen atomic distances both along and across the c-GaN backbone ridges. The geometry of these distances is illustrated in Fig. 5(b).

From the trends in bond-length/atomic distance summarized in Table I, it is clear that the presence of the excess carriers has little effect on the local geometry of the transition state if the conduction band resonant levels remain unoccupied. However, with occupation of the resonant level(s) by excess electrons, significant local expansion around the Ga atom occurs. Essentially, the nitrogen atoms below the swinging Ga atom sink lower and further away from the Ga atom, allowing for a more open pathway for the motion of the Ga atom. Accompanying these geometric changes is a lowering of the resonant state eigenvalues relative to the band edge of order 0.4–1.0 eV, depending upon whether one or both resonant levels are occupied. In general, occupation of localized and quasi-localized levels typically leads to lattice relaxation. On the other hand, moving an electron from one delocalized level to another has little effect on the defect geometry. Although, as noted above, we only explicitly consider the neutral state of the Ga vacancy (i.e., there are no changes to the midgap levels), our results indicate that occupation of quasi-localized resonant levels can lead to an effective change in the charge state of the defect.

The results plotted in Fig. 5 allow us to conclude that, as excess electrons in the conduction bands enter and exit resonances, the migration-energy landscape becomes dynamic and undulatory, with dips and rises that can be encountered during migration attempts. We can identify an alternative role of resonances enhancing defect migration by identifying the key factor controlling the lifetime of an electron in a defect-induced resonance. Consider an electron in the lowest-energy resonance in the conduction bands. Its lifetime is controlled by the probability of the electron dropping into a lower-energy state, namely, either a Bloch state in the bands between the resonance and the bottom of the conduction bands or a defect bound state in the energy gap. Such transition probabilities are proportional to the square of matrix elements between the initial and final states. It is clear that such matrix elements are largest for the transition to a bound state when both initial and final states have a degree of localization about the defect. Cross sections for such transitions can be calculated,[70,71] but are beyond the scope of this paper. The transition energy, which can be several eV, is dissipated into lattice vibrations, predominantly those of the defect atoms, a form of local heating that can boost the defect migration rate or overcome the migration barrier altogether. Hence, in the presence of excess carriers, defect resonances can have a large impact on defect migration. Similarly, during the H release from passivated defects by inelastic scattering of hot electrons,[72] a transition from a Bloch state to a resonance would have a higher probability of occurring via multiphonon processes, as it is analogous to a Bloch-carrier capture by a bound defect, compared with a Bloch-state-to-Bloch-state transition.

The process we described above can be further enhanced if excess holes in the valence bands also have opportunities to occupy resonances and then transition to a bound state. Thus, either an excess electron or an excess hole in a respective resonance being captured at a defect bound state can significantly enhance defect migration. A consecutive electron and hole capture, i.e., a recombination event by carriers in resonances can have an even bigger impact on the migration process.

IV. DEFECT MULTIPLICATION AND VOID FORMATION

Often, during catastrophic failure of a device by single-ion events, pits and voids form.[34–37] The formation of pits and voids can ultimately be attributed to the sheer amount of energy that is dissipated by the lattice, namely, Joule heating generated by the voltage and the charge flowing along the ion path. TCAD simulations[33] have shown that an increase in the ion LET or an increase in the voltage enhances degradation and failure. Furthermore, the presence of large concentrations of excess carriers, augmented by resonances in the band continua at DD along the ion path, provides additional mechanisms for energy transfer to the lattice, especially in the regime of lower voltages and LETs. However, atomistic mechanisms for the pit and void formation have not been explored so far. Though piezoelectric stress relief is a partial culprit, it is not the major cause as its effect on lowering defect migration barriers has been shown to be small.[73] Other factors have also been invoked at a phenomenological level.[36,37]

To investigate how the formation of a void may initiate, we look at a microscopic mechanism that we term the defect-multiplication process. Fundamentally, we envision a cascading process where a pre-existing vacancy or the knockout of an atom by an ion strike lowers the energy required for successive removal of neighboring atoms. Typically, the adjacent atoms are opposite in type to the missing atom; however, as the void enlarges, either type of additional vacancies could occur. A schematic diagram of the defect multiplication process in a simple binary compound is shown in Fig. 6.

To examine this process in detail, we first determine the energy cost to remove a Ga or a N from the perfect GaN lattice and place it at an interstitial site, i.e., the energy cost of a FP, for comparison with the energy costs to similarly remove atoms adjacent to the original vacant site. We find that, for a N FP, the lowest-energy stable configuration for the ejected N is a neighboring split-interstitial site. On the other hand, in the case of Ga ejection, the nearest stable site is a neighboring tetrahedral interstitial site with N coordination, which is not normally the lowest-energy interstitial configuration. The interstitial can, of course, later separate from the vacancy cluster. The initial ejection energies, i.e., the energy differences between the pristine material and the above-described FPs are 10.0 eV for Ga and 7.5 eV for N. The full energy barrier for the creation process calculated using the nudged-elastic band method is 10.5 eV for Ga and 7.7 eV for N. The differences in ejection and barrier energies were found to be similarly small in other test cases. Furthermore, since the energy barriers for the recombination of such FPs are small, additional small amounts of energy are needed for the ejected interstitial to overcome migration barriers and migrate to distant sites. These migration energies are of order 1–2 eV, depending on the charge state of the ejected interstitial.[74] Therefore, for comparison with the energies to remove atoms adjacent to the initial vacancy, we shall leave out migration

18 May 2024 05:49:24

© Author(s) 2024

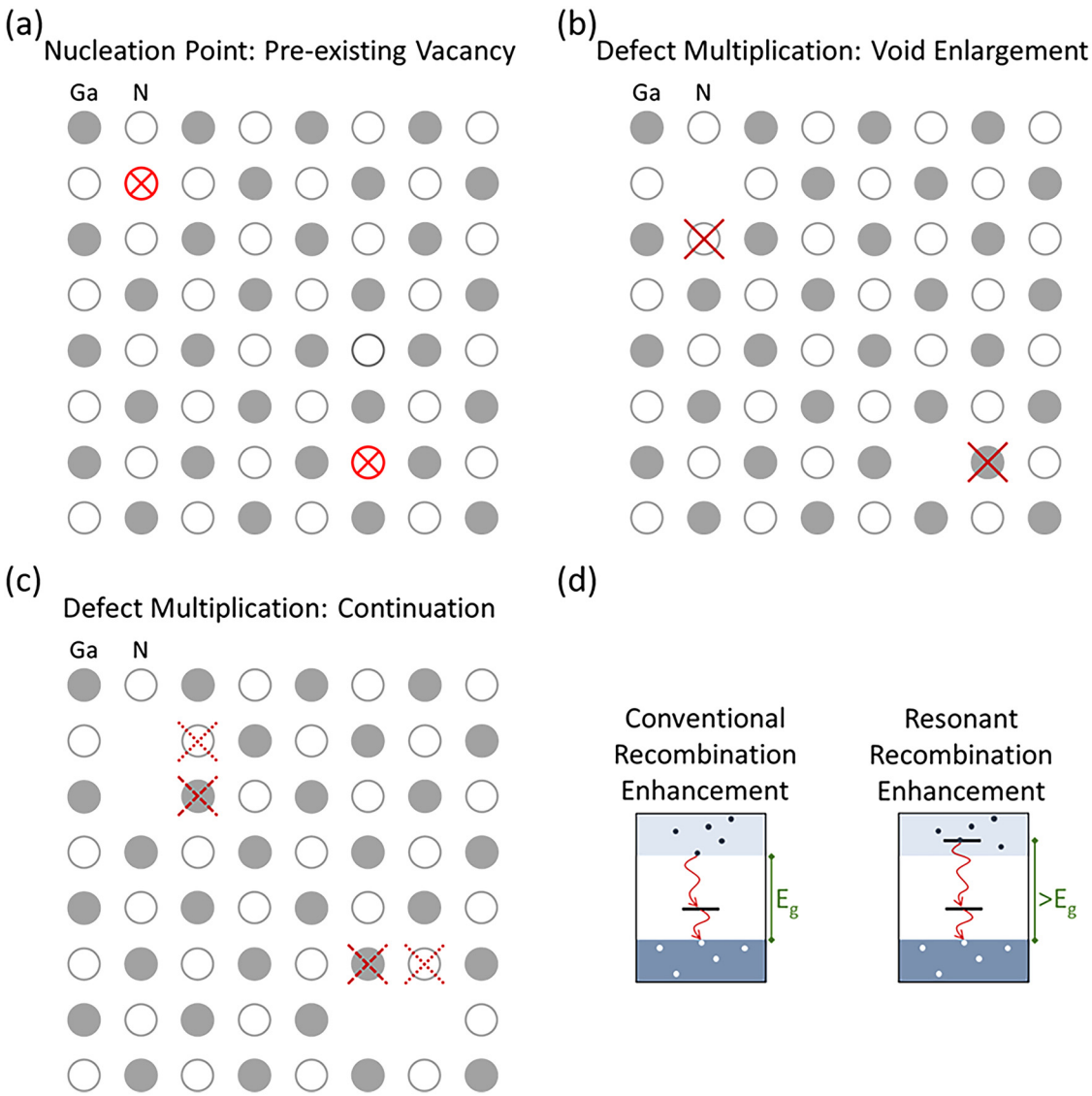

FIG. 6. (a)–(c) Schematic diagrams representing the general process for defect multiplication starting from an initial vacancy of either type. (a) An initial pre-existing vacancy (either from processing or displaced during an ion strike) provides a nucleation point and may occur at either lattice site. (b) From there, the energy cost to remove an adjacent atom of the opposite type can occur at a lower energy cost. (c) Continuation of the void enlargement can occur through many possible pathways involving either atomic species. (d) In the presence of significant numbers of electron–hole pairs, the energy for an atom to be removed from its lattice site at the nanovoid rim to a distant interstitial site may be provided either through conventional recombination enhancement providing an E_g of energy per recombination event or as mediated by resonant levels which can provide greater than an E_g of energy per recombination, or by inelastic scattering events.

energies and use 10.0 and 7.5 eV for Ga and N FPs in a perfect GaN lattice, respectively (Fig. 7).

The energies for FP creation in the pristine material are quite high, of order three and two times the bandgap of GaN, for the Ga and N FP, respectively. DFT-based molecular-dynamics simulations and experiments find that the threshold for an energetic ion to knock an atom out of its lattice site in a crystal is actually larger because the knocked-out atom does not simply migrate along a migration barrier to a far enough point to avoid return to its original site. Instead, a knocked-out atom scatters off other atoms and transfers energy to them in order to reach a far enough stable site.[41] However, if we calculate the energetics under the assumption of a pre-existing Ga vacancy or N vacancy, the energy required to remove additional atoms drops significantly as illustrated in Fig. 7. The figure makes clear that there is a path for the sequential removal of atoms to enlarge a nanovoid at energy costs of order the

18 May 2024 05:49:24

© Author(s) 2024

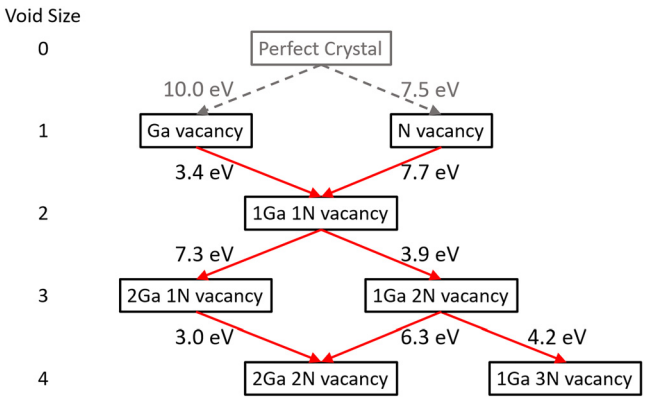

FIG. 7. Energetics for vacancy void enlargement in c-GaN as a function of void size from initial vacancy to four adjacent vacancies. Each energy represents the approximate energetic cost to eject an additional Ga or N atom to enlarge the void. See discussion in the text.

bandgap per atom or slightly larger if we include the migration barriers discussed above.

The results presented in Fig. 7 and the corresponding trends allow us to draw several conclusions. First, removal of one atomic species generally lowers the energetic cost for the removal of the opposite type of atom. This feature can be seen immediately as a pre-existing Ga vacancy can lower the removal energy of N by ~4 eV, from 7.5 to 3.4 eV, while a pre-existing N vacancy can lower the removal of a Ga atom by 3.3 eV, from 10.0 to 7.7 eV. This trend is fairly general in that removal of one atomic species benefits the removal of the other atomic species. Furthermore, as the void enlarges, the energy for N removal drops to be similar in energy to the GaN bandgap. While N removal is generally lower in energy than Ga removal, enlargement of the void by several nitrogen atoms can significantly lower the energy for Ga removal. For example, removal of two N atoms around a pre-existing Ga vacancy lowers the removal energy of the second Ga atom to 6.3 eV. These results suggest that the void can enlarge from an initial Ga vacancy by removal of several nitrogen atoms and then subsequently an additional Ga atom, repeating the process as energy becomes available.

To date, limited work on multivacancy structures in GaN exists. From a thermodynamic point of view, the divacancy in n-type w-GaN is always less stable than the gallium vacancy for N-rich conditions or the nitrogen vacancy for Ga-rich conditions,[75,76] while trivacancies (2Ga and 1N vacancy) are unstable for p-type w-GaN with a similar formation to the divacancy for n-type w-GaN.[77] Part of this results from the tendency for vacancy-antisite and vacancy-substitutional-impurity complexes to form instead. In c-GaN, divacancies and trivacancies (either the 2Ga 1N vacancy or 1Ga 2N vacancy) only have a single type of structure for those removed atoms due to the crystal symmetry. Structurally dissimilar arrangements only occur when dealing with four or more removed atoms. In the current work, this only occurs for the 2Ga-2N vacancy where either a compact ring-like structure or extended chain-like structures can form. Since these only appear in the context of having the displaced Ga or N atom nearby (i.e., going from line 3 to the left side of line 4 in Fig. 7), we find that the initial formation of chain-like structures tends to happen more readily. We note, however, that these are not the final, stable quad-vacancy type structures and would still require further diffusion of the ejected atom. Prior work on multivacancies in silicon[78–80] indicates that the more compact ring-like structures are often more stable, but that chains can also form. However, in the case of defect multiplication during ion irradiation, both types of structures are likely to occur after the ejected atoms diffuse away since the multi-vacancy formation process does not occur under thermodynamic equilibrium conditions.

The result that step-by-step defect multiplication (void enlargement) requires energies of order the material's bandgap or slightly larger is significant as, in the presence of excess carriers even under TID conditions, electron–hole recombination mediated by defect levels in the energy gap releases an amount of energy of order the bandgap. Resonance-enhanced recombination can release even larger amounts of energy. The released energy is taken up primarily by local phonons that can affect the removal of atoms for void enlargement. Though phonon-mediated processes can be relatively slow, continuous exposure to ionizing radiation and back-to-back recombination processes can lead to the formation of nanovoids that can trap charge and complicate the analysis of threshold voltage shifts and transconductance degradation along with the activation of pre-existing passivated vacancies, antisite defects, or impurities.[12,15] On the other hand, in the case of energetic heavy ions and large applied voltages, the ion's LET and Joule heating can provide plenty of energy more directly to induce nanovoid formation along the ion's path. As the energy is dissipated along the ion path, ion-generated vacancies can easily migrate, and either undergo growth or attach themselves to another void. These processes can lead to a formation of a conducting "defect nanowire." Secondary knockout atoms can lead to an enlargement of the nanowire diameter. As we deduced earlier in this paper, displacement damage, including nanovoids, is accompanied by resonances that help channel the excess-carrier currents. The combination of these phenomena can make the case for a major DD role in SEE soft breakdowns. Under sufficiently high voltages, runaway void growth could be responsible for explosive hard breakdowns of devices, featuring pits and voids.[34–37]

V. CONCLUSIONS

In summary, we have employed DFT calculations to explore several atomic-scale mechanisms, including the role of rather exotic quantum effects such as defect-induced resonances in the band continua of semiconductors that can participate in or even play a dominant role in radiation- and hot-electron-induced device degradation and failure. Common themes are (a) the generation of excess electrons and holes by radiation or simply the presence of hot carriers, (b) the existence of defect-induced resonances in band continua that can evolve and multiply during displacement damage by energetic ions, and (c) defect multiplication at vacancies (nanovoid formation) that can occur with significantly reduced energy compared with Frenkel-pair formation in perfect crystals. Electrons

18 May 2024 05:49:24

© Author(s) 2024

or holes in resonances can be more effective in enhancing defect dynamics because their capture by one of the defect energy levels in the bandgap via multiphonon processes is more efficient than the capture of Bloch electrons. Thus, nanovoids can form and play a role in TID and hot-electron device degradation. On the other hand, energetic-ion-induced displacement damage, enhanced by defect multiplication and decorated by evolving and multiplying resonances, can provide efficient pathways for excess-carrier current, which, driven by high voltages can affect soft breakdowns and even hard breakdowns, possible by explosive void growth that can lead to pits and voids. Though the theoretical evidence for the above processes is substantial, experimental validation remains an open question at this stage.

Although the focus at present has been on c-GaN, we expect that the same behaviors observed here would also occur in other materials with some caveats. In particular, the spectrum of resonances in both the conduction and valence bands during defect migration assuredly varies from defect type to defect type and from material to material. A scarcity of resonances, if it ever occurs, would of course reduce the impact that we described in this paper. Similarly, in some wide-gap semiconductors, the energetic cost of void growth may be much higher than in others, as compared with the material's bandgap. Thus, resistance to void growth emerges as a criterion for rating a material's radiation resistance, especially if it can be validated by carefully designed experiments. Such phenomena are, of course, expected to occur by resonances in the valence bands when occupied by holes. The presence or relative absence of resonances associated with defects may also be an indicator of the relative radiation resistance of each material. Similarly, for defect multiplication and the generation of voids, the pertinent lowering of the atom-ejection energies may be an indicator of the relative radiation resistance of each material.

ACKNOWLEDGMENTS

This work was supported by the Air Force Office of Scientific Research Center of Excellence on Radiation Effects via Grant No. FA9550-22-1-0012 and by the McMinn Endowment at Vanderbilt University. Computational support was provided by the Department of Defense's High Performance Computing Modernization Program (HPCMP).

AUTHOR DECLARATIONS

Conflict of Interest

The authors have no conflicts to disclose

Author Contributions

Andrew O'Hara: Formal analysis (equal); Investigation (equal); Methodology (equal); Writing – original draft (equal). **Ronald D. Schrimpf:** Formal analysis (equal); Funding acquisition (equal); Validation (equal); Writing – review & editing (equal). **Daniel M. Fleetwood:** Conceptualization (equal); Formal analysis (equal); Funding acquisition (equal); Writing – review & editing (equal). **Sokrates T. Pantelides:** Conceptualization (equal); Formal analysis (equal); Funding acquisition (equal); Methodology (equal); Project administration (equal); Supervision (equal); Writing – review & editing (equal).

DATA AVAILABILITY

Raw data were generated at the HPCMP large scale facility. Derived data supporting the findings of this study are available from the corresponding author upon reasonable request.

REFERENCES

[1]S. M. Sze, *Physics of Semiconductor Devices*, 2nd ed. ((John Wiley & Sons, Inc., New York, 1981).
[2]W. Shockley, "Problems related to p-n junctions in silicon," Solid State Electron. **2**, 35 (1961).
[3]S. T. Pantelides, D. G. Walker, M. Reaz, M. V. Fischetti, and R. D. Schrimpf, "The foundations of Shockley's equation for the average electron–hole-pair creation energy in semiconductors," Appl. Phys. Lett. **121**, 042104 (2022).
[4]D. O. Nielsen, C. G. Van de Walle, S. T. Pantelides, R. D. Schrimpf, D. M. Fleetwood, and M. V. Fischetti, "First-principles approach to closing the 10–100 eV gap for charge-carrier thermalization in semiconductors," Phys. Rev. B **108**, 155203 (2023).
[5]F. B. McLean, "A framework for understanding radiation-induced interface states in SiO_2 MOS structures," IEEE Trans. Nucl. Sci. **27**, 1651 (1980).
[6]D. M. Fleetwood, P. S. Winokur, R. A. Reber, T. L. Meisenheimer, J. R. Schwank, M. R. Shaneyfelt, and L. C. Riewe, "Effects of oxide traps, interface traps, and 'border traps' on metal-oxide-semiconductor devices," J. Appl. Phys. **73**, 5058 (1993).
[7]S. N. Rashkeev, D. M. Fleetwood, R. D. Schrimpf, and S. T. Pantelides, "Defect generation by hydrogen at the Si-SiO_2 interface," Phys. Rev. Lett. **87**, 165506 (2001).
[8]D. M. Fleetwood, "Effects of hydrogen transport and reactions on microelectronics radiation response and reliability," Microelectron. Reliab. **42**, 523 (2002).
[9]T. R. Oldham and F. B. McLean, "Total ionizing dose effects in MOS oxides and devices," IEEE Trans. Nucl. Sci. **50**, 483 (2003).
[10]S. T. Pantelides, L. Tsetseris, S. N. Rashkeev, X. J. Zhou, D. M. Fleetwood, and R. D. Schrimpf, "Hydrogen in MOSFETs—A primary agent of reliability issues," Microelectron. Reliab. **47**, 903 (2007).
[11]S. T. Pantelides, L. Tsetseris, M. J. Beck, S. N. Rashkeev, G. Hadjisavvas, I. G. Batyrev, B. R. Tuttle, A. G. Marinopoulos, X. J. Zhou, D. M. Fleetwood, and R. D. Schrimpf, "Performance, reliability, radiation effects, and aging issues in microelectronics—From atomic-scale physics to engineering-level modeling," Solid State Electron. **54**, 841 (2010).
[12]S. T. Pantelides, Y. Puzyrev, X. Shen, T. Roy, S. DasGupta, B. R. Tuttle, D. M. Fleetwood, and R. D. Schrimpf, "Reliability of III–V devices – The defects that cause the trouble," Microelectron. Eng. **90**, 3 (2012).
[13]X. Shen, Y. S. Puzyrev, D. M. Fleetwood, R. D. Schrimpf, and S. T. Pantelides, "Quantum mechanical modeling of radiation-induced defect dynamics in electronic devices," IEEE Trans. Nucl. Sci. **62**, 2169 (2015).
[14]D. M. Fleetwood, "Total-ionizing-dose effects, border traps, and 1/f noise in emerging MOS technologies," IEEE Trans. Nucl. Sci. **67**, 1216 (2020).
[15]D. M. Fleetwood, E. X. Zhang, R. D. Schrimpf, and S. T. Pantelides, "Radiation effects in AlGaN/GaN HEMTs," IEEE Trans. Nucl. Sci. **69**, 1105 (2022).
[16]M. Sparks, D. L. Mills, R. Warren, T. Holstein, A. A. Maradudin, L. J. Sham, E. Loh, and D. F. King, "Theory of electron-avalanche breakdown in solids," Phys. Rev. B **24**, 3519 (1981).
[17]T. F. Wrobel, F. N. Coppage, G. L. Hash, and A. J. Smith, "Current induced avalanche in epitaxial structures," IEEE Trans. Nucl. Sci. **32**, 3991 (1985).
[18]T. F. Wrobel, "On heavy ion induced hard-errors in dielectric structures," IEEE Trans. Nucl. Sci. **34**, 1262 (1987).
[19]T. A. Fischer, "Heavy-ion-induced, gate-rupture in power MOSFETs," IEEE Trans. Nucl. Sci. **34**, 1786 (1987).
[20]S. Kuboyama, S. Matsuda, T. Kanno, and T. Hirose, "Single event burnout of power MOSFETs caused by nuclear reactions with heavy ions," IEEE Trans. Nucl. Sci. **41**, 2210 (1994).

18 May 2024 05:49:24

© Author(s) 2024

[21]G. H. Johnson, J. M. Palau, C. Dachs, K. F. Galloway, and R. D. Schrimpf, "A review of the techniques used for modeling single-event effects in power MOSFETs," IEEE Trans. Nucl. Sci. **43**, 546 (1996).
[22]F. W. Sexton, "Destructive single-event effects in semiconductor devices and ICs," IEEE Trans. Nucl. Sci. **50**, 603 (2003).
[23]S. Kuboyama, A. Maru, H. Shindou, N. Ikeda, T. Hirao, H. Abe, and T. Tamura, "Single-event damages caused by heavy ions observed in AlGaN/GaN HEMTs," IEEE Trans. Nucl. Sci. **58**, 2734 (2011).
[24]F. W. Sexton, D. M. Fleetwood, M. R. Shaneyfelt, P. E. Dodd, G. L. Hash, L. P. Schanwald, R. A. Loemker, K. S. Krisch, M. L. Green, B. E. Weir, and P. J. Silverman, "Precursor ion damage and angular dependence of single event gate rupture in thin oxides," IEEE Trans. Nucl. Sci. **45**, 2509 (1998).
[25]F. W. Sexton, D. M. Fleetwood, M. R. Shaneyfelt, P. E. Dodd, and G. L. Hash, "Single event gate rupture in thin gate oxides," IEEE Trans. Nucl. Sci. **44**, 2345 (1997).
[26]L. W. Massengill, B. K. Choi, D. M. Fleetwood, R. D. Schrimpf, K. F. Galloway, M. R. Shaneyfelt, T. L. Meisenheimer, P. E. Dodd, J. R. Schwank, Y. M. Lee, R. S. Johnson, and G. Lucovsky, "Heavy-ion-induced breakdown in ultra-thin gate oxides and high-k dielectrics," IEEE Trans. Nucl. Sci. **48**, 1904 (2001).
[27]T. F. Wrobel and D. E. Beutler, "Solutions to heavy ion induced avalanche burnout in power devices," IEEE Trans. Nucl. Sci. **39**, 1636 (1992).
[28]D. R. Ball, K. F. Galloway, R. A. Johnson, M. L. Alles, A. L. Sternberg, A. F. Witulski, R. A. Reed, R. D. Schrimpf, J. M. Hutson, and J.-M. Lauenstein, "Effects of breakdown voltage on single-event burnout tolerance of high-voltage SiC power MOSFETs," IEEE Trans. Nucl. Sci. **68**, 1430 (2021).
[29]S. Kuboyama, S. Matsuda, M. Nakajima, T. Kanno, and T. Ishii, "Numerical analysis of single event burnout of power MOSFETs," IEEE Trans. Nucl. Sci. **40**, 1872 (1993).
[30]J. L. Titus and C. F. Wheatley, "Experimental studies of single-event gate rupture and burnout in vertical power MOSFETs," IEEE Trans. Nucl. Sci. **43**, 533 (1996).
[31]M. Allenspach, C. Dachs, G. H. Johnson, R. D. Schrimpf, E. Lorfevre, J. M. Palau, J. R. Brews, K. F. Galloway, J. L. Titus, and C. F. Wheatley, "SEGR and SEB in n-channel power MOSFETs," IEEE Trans. Nucl. Sci. **43**, 2927 (1996).
[32]J. L. Titus, "An updated perspective of single event gate rupture and single event burnout in power MOSFETs," IEEE Trans. Nucl. Sci. **60**, 1912 (2013).
[33]D. R. Ball, J. M. Hutson, A. Javanainen, J.-M. Lauenstein, K. F. Galloway, R. A. Johnson, M. L. Alles, A. L. Sternberg, B. D. Sierawski, A. F. Witulski, R. A. Reed, and R. D. Schrimpf, "Ion-induced energy pulse mechanism for single-event burnout in high-voltage SiC power MOSFETs and junction barrier Schottky diodes," IEEE Trans. Nucl. Sci. **67**, 22 (2020).
[34]J. Joh and J. A. del Alamo, "Critical voltage for electrical degradation of GaN high-electron mobility transistors," IEEE Electron Device Lett. **29**, 287 (2008).
[35]U. Chowdhury, J. L. Jimenez, C. Lee, E. Beam, P. Saunier, T. Balistreri, S.-Y. Park, T. Lee, J. Wang, M. J. Kim, J. Joh, and J. A. del Alamo, "TEM observation of crack- and pit-shaped defects in electrically degraded GaN HEMTs," IEEE Electron Device Lett. **29**, 1098 (2008).
[36]S.-Y. Park, T.-H. Lee, and M.-J. Kim, "Correlation between physical defects and performance in AlGaN/GaN high electron mobility transistor devices," IEEE Trans. Electr. Electron. Mater. **11**, 49 (2010).
[37]P. Makaram, J. Joh, J. A. del Alamo, T. Palacios, and C. V. Thompson, "Evolution of structural defects associated with electrical degradation in AlGaN/GaN high electron mobility transistors," Appl. Phys. Lett. **96**, 233509 (2010).
[38]M. J. Beck, R. Hatcher, R. D. Schrimpf, D. M. Fleetwood, and S. T. Pantelides, "Quantum mechanical description of displacement damage formation," IEEE Trans. Nucl. Sci. **54**, 1906 (2007).
[39]M. J. Beck, B. R. Tuttle, R. D. Schrimpf, D. M. Fleetwood, and S. T. Pantelides, "Atomic displacement effects in single-event gate rupture," IEEE Trans. Nucl. Sci. **55**, 3025 (2008).
[40]R. M. Cadena, D. R. Ball, E. X. Zhang, S. Islam, A. Senarath, M. W. McCurdy, E. Farzana, J. S. Speck, N. Karom, A. O'Hara, B. R. Tuttle, S. T. Pantelides, A. F. Witulski, K. F. Galloway, M. L. Alles, R. A. Reed, D. M. Fleetwood, and R. D. Schrimpf, "Low-energy ion-induced single-event burnout in gallium oxide Schottky diodes," IEEE Trans. Nucl. Sci. **70**, 363 (2023).
[41]B. R. Tuttle, N. J. Karom, A. O'Hara, R. D. Schrimpf, and S. T. Pantelides, "Atomic-displacement threshold energies and defect generation in irradiated β-Ga_2O_3: A first-principles investigation," J. Appl. Phys. **133**, 015703 (2023).
[42]A. M. Stoneham, *Theory of Defects in Solids* (Oxford University Press, Oxford, UK, 2001).
[43]A. M. Stoneham, "Non-radiative transitions in semiconductors," Rep. Prog. Phys. **44**, 1251 (1981).
[44]J. Bourgoin and J. Corbett, "A new mechanism for interstitial migration," Phys. Lett. A **38**, 135 (1972).
[45]G.D. Watkins, in *Lattice Defects Semiconductors: Invited and Contributed Papers from International Conference Held in Freiburg, 22-25 July 1974*, edited by F. A. Huntley (Institute of Physics, Bristol, 1975), p. 23.
[46]J. D. Weeks, J. C. Tully, and L. C. Kimerling, "Theory of recombination-enhanced defect reactions in semiconductors," Phys. Rev. B **12**, 3286 (1975).
[47]J. R. Troxell, A. P. Chatterjee, G. D. Watkins, and L. C. Kimerling, "Recombination-enhanced migration of interstitial aluminum in silicon," Phys. Rev. B **19**, 5336 (1979).
[48]G. A. Baraff, M. Schluter, and G. Allan, "Theory of enhanced migration of interstitial aluminum in silicon," Phys. Rev. Lett. **50**, 739 (1983).
[49]S. T. Pantelides, A. Oshiyama, R. Car, and P. J. Kelly, "Theory of electronically stimulated defect migration in semiconductors," Phys. Rev. B **30**, 2260 (1984).
[50]S.-Z. Yang, W. Sun, Y.-Y. Zhang, Y. Gong, M. P. Oxley, A. R. Lupini, P. M. Ajayan, M. F. Chisholm, S. T. Pantelides, and W. Zhou, "Direct cation exchange in monolayer MoS_2 via recombination-enhanced migration," Phys. Rev. Lett. **122**, 106101 (2019).
[51]J. Bernholc, N. O. Lipari, and S. T. Pantelides, "Self-consistent method for point defects in semiconductors: Application to the vacancy in silicon," Phys. Rev. Lett. **41**, 895 (1978).
[52]G. Kresse and J. Furthmüller, "Efficient iterative schemes for *ab initio* total-energy calculations using a plane-wave basis set," Phys. Rev. B **54**, 11169 (1996).
[53]P. Blöchl, "Projector augmented-wave method," Phys. Rev. B **50**, 17953 (1994).
[54]G. Kresse and D. Joubert, "From ultrasoft pseudopotentials to the projector augmented-wave method," Phys. Rev.B **59**, 1758 (1999).
[55]J. P. Perdew, K. Burke, and M. Ernzerhof, "Generalized gradient approximation made simple," Phys. Rev. Lett. **77**, 3865 (1996).
[56]G. Henkelman and H. Jonsson, "Improved tangent estimate in the nudged elastic band method for finding minimum energy paths and saddle points," J. Chem. Phys. **113**, 9978 (2000).
[57]G. Henkelman, B. P. Uberuaga, and H. Jonsson, "A climbing image nudged elastic band method for finding saddle points and minimum energy paths," J. Chem. Phys. **113**, 9901 (2000).
[58]G. D. Watkins, *Radiation in Damage Semiconductors* (Dunod, Paris, 1964).
[59]E. T. Whittaker and G. N. Watson, *A Course of Modern Analysis*, 4th ed. (Cambridge University Press, 1927).
[60]A. S. Eddington, "Eigenvalues and Whittaker's function," Nature **120**, 117 (1927).
[61]Y. Matsushita, S. Furuya, and A. Oshiyama, "Floating electron states in covalent semiconductors," Phys. Rev. Lett. **108**, 246404 (2012).
[62]Y. Matsushita and A. Oshiyama, "Interstitial channels that control band gaps and effective masses in tetrahedrally bonded semiconductors," Phys. Rev. Lett. **112**, 136403 (2014).
[63]F. Nanataki, K. Shiraishi, J. Iwata, Y. Matsushita, and A. Oshiyama, "Atomic and electronic structures of nitrogen vacancies in silicon nitride: Emergence of floating gap states," Phys. Rev. B **106**, 155201 (2022).
[64]F. Wegner, "Inverse participation ratio in 2+ϵ dimensions," Z. Phys. B **36**, 209 (1980).
[65]F. Evers and A. D. Mirlin, "Fluctuations of the inverse participation ratio at the Anderson transition," Phys. Rev. Lett. **84**, 3690 (2000).
[66]R. J. Bell and P. Dean, "The structure of vitreous silica: Validity of the random network theory," Philos. Mag. **25**, 1381 (1972).
[67]S. I. Simdyankin, S. R. Elliott, Z. Hajnal, T. A. Niehaus, and T. Frauenheim, "Simulation of physical properties of the chalcogenide glass As_2S_3 using a density-functional-based tight-binding method," Phys. Rev. B **69**, 144202 (2004).

18 May 2024 05:49:24

© Author(s) 2024

[68]J.D. Wrbanek, S.Y. Wrbanek, G.C. Fralick, and L. Chen, "Micro-fabricated solid-state radiation detectors for active personal dosimetry," NASA Report No. NASA/TM 214674, 2007.
[69]J. L. Barth, C. S. Dyer, and E. G. Stassinopoulos, "Space, atmospheric, and terrestrial radiation environments," IEEE Trans. Nucl. Sci. **50**, 466 (2003).
[70]A. Alkauskas and Q. Yan, and C.G. Van de Walle, "First-principles theory of nonradiative carrier capture via multiphonon emission," Phys. Rev. B **90**, 075202 (2014).
[71]G. D. Barmparis, Y. S. Puzyrev, X.-G. Zhang, and S. T. Pantelides, "Theory of inelastic multiphonon scattering and carrier capture by defects in semiconductors: Application to capture cross sections," Phys. Rev. B **92**, 214111 (2015).
[72]S. Mukherjee, Y. Puzyrev, J. Chen, D. M. Fleetwood, R. D. Schrimpf, and S. T. Pantelides, "Hot-carrier degradation in GaN HEMTs due to substitutional iron and its complexes," IEEE Trans. Electron Devices **63**, 1486 (2016).
[73]K. H. Warnick, Y. Puzyrev, T. Roy, D. M. Fleetwood, R. D. Schrimpf, and S. T. Pantelides, "Room-temperature diffusive phenomena in semiconductors: The case of AlGaN," Phys. Rev. B **84**, 214109 (2011).
[74]S. Limpijumnong and C. Van de Walle, "Diffusivity of native defects in GaN," Phys. Rev. B **69**, 035207 (2004).
[75]M. G. Ganchenkova and R. M. Nieminen, "Nitrogen vacancies as major point defects in gallium nitride," Phys. Rev. Lett. **96**, 196402 (2006).
[76]Y. S. Puzyrev, T. Roy, M. Beck, B. R. Tuttle, R. D. Schrimpf, D. M. Fleetwood, and S. T. Pantelides, "Dehydrogenation of defects and hot-electron degradation in GaN high-electron-mobility transistors," J. Appl. Phys. **109**, 034501 (2011).
[77]Y. Gohda and A. Oshiyama, "Stabilization mechanism of vacancies in group-III nitrides: Exchange splitting and electron transfer," J. Phys. Soc. Jpn. **79**, 083705 (2010).
[78]S. T. Pantelides, I. Ivanov, M. Scheffler, and J. P. Vigneron, "Multivacancies, interstitials, and self-interstitial migration in silicon," Physica B + C **116**, 18 (1983).
[79]D. J. Chadi and K. J. Chang, "Magic numbers for vacancy aggregation in crystalline Si," Phys. Rev. B **38**, 1523 (1988).
[80]T. Akiyama and A. Oshiyama, "First-principles study of hydrogen incorporation in multivacancy in silicon," J. Phys. Soc. Jpn. **70**, 1627 (2001).

18 May 2024 05:49:24

© Author(s) 2024